Dynamical properties of two-dimensional quasicrystals

J. A. Ashraff
Department of Theoretical Physics, Oxford University, 1 Keble Road, Oxford, OX1 3NP, United Kingdom

J-M. Luck
Department of Theoretical Physics, Oxford University, 1 Keble Road, Oxford, OX1 3NP, United Kingdom and Service de Physique Théorique, Centre d'Etudes Nucléaires de Saclay, 91191 Gif-sur-Yvette CEDEX, France

R. B. Stinchcombe
Department of Theoretical Physics, Oxford University, 1 Keble Road, Oxford, OX1 3NP, United Kingdom
(Received 13 March 1989; revised manuscript received 4 October 1989)

Electron and phonon spectra, densities and integrated densities of states, and dynamic-response functions are investigated for a variety of two-dimensional (2D) quasicrystals. The dynamical properties of a Fibonacci chain, extended both periodically and quasiperiodically into a second dimension, are obtained using an exact convolution relationship involving only one-dimensional quantities. For a particular on-site model we find two successive transitions in the spectrum of the quasiperiodically extended Fibonacci chain (2D Fibonacci quasilattice) as a function of coupling strength: from finite to infinite band number and from finite to zero total bandwidth. The periodically extended Fibonacci chain (Fibonacci superlattice) always has a finite band number and nonzero total bandwidth. Furthermore, in each case we find the plateaux in the integrated density of states to follow a gap-labeling rule, as is the case in one dimension. We also present for the first time a study of the spectrum of a particular 2D Penrose lattice generated via the Robinson tiling approach. Our study of the spectrum is made by diagonalizing the matrices of finite-size samples, our results indicating that the gap number is always finite, irrespective of the coupling strengths. Plots of the integrated electronic and vibrational densities of states indicate a similar gap-labeling rule as was found for the 2D Fibonacci superlattice and quasilattice. Surface plots of the full wave-vector and frequency-dependent response functions (dynamic-structure factor) are given for both the 2D Fibonacci and Penrose lattices, and show very rich structure. That for the Fibonacci quasilattice can be interpreted by comparison with an exact analytic expression obtained in the equal-coupling limit, which indicates that the response is strongly peaked along well-defined curves in the frequency-wave vector plane, unlike that for the Penrose lattice, which shows no apparent regularity, except in the long-wavelength limit.

I. INTRODUCTION

Since the discovery [1] in 1984 of systems exhibiting sharp diffraction patterns with a symmetry inconsistent with a perfect crystalline order, and their interpretation[2,3] as quasiperiodic lattices ("quasicrystals"), many theoretical studies have investigated the static[3–8] (e.g., magnetic) and dynamical[8] properties of quasicrystal models. While the dynamical studies have lagged behind the static ones, a clear picture is emerging of the dynamical behavior of one-dimensional quasicrystals, particularly the Fibonacci chain, following its formulation in terms of a trace map.[9,10] In particular, the spectrum and the integrated density of states of the Fibonacci chain have been investigated[9,11,12] and, among other studies, the multifractal aspects have been characterized.[13,14] More recently,[15,16] the development of an exact decimation rescaling technique for the Fibonacci chain has allowed direct and accurate determinations of density or integrated density of states, in addition to the full dynamic response function.

The present paper is concerned with the dynamical properties of two-dimensional (2D) quasicrystals. The systems studied include a particular Penrose lattice[17–19] as well as higher-dimensional variants of the Fibonacci chain. These variants involve the extension of the chain into a second dimension in either a periodic manner, yielding a Fibonacci superlattice,[20] or according to a second Fibonacci sequence, yielding a Fibonacci (isotropic or anisotropic) quasilattice.[21,22] The particular Penrose lattice we have chosen to study is generated via a recursive construction due to Robinson,[4,18,19] leading to a succession of finite-size Penrose lattices having fixed triangular boundaries, and this avoids most irregularities in size dependencies. All previous studies of the electronic and vibrational properties[23–29] have focused only on those Penrose lattices composed of either two types of rhombs or darts and kites. The Penrose lattice we have considered is in a different local isomorphism class[30] to these and hence is expected to have different dynamical properties. Indeed, it is evident that a Penrose lattice composed of Robinson tiles is a much more highly connected and rigid structure than those composed of darts and kites and of rhombs, and so one would expect its

spectrum to have fewer gaps.

The spectrum of the one-dimensional Fibonacci-chain quasicrystal is known rigorously to be a Cantor set of zero Lebesgue measure for any value of the on-site potential.[31] However, the additional degrees of freedom present in higher dimensions may lead one to conjecture that fewer, or possibly no gaps, will appear in the spectrum of the higher-dimensional generalizations. For a small enough coupling strength along one direction, the lattice is essentially composed of noninteracting linear chains, and so we would expect a spectrum not unlike that obtained in one dimension. It is thus not unreasonable to conjecture that as a function of coupling strength, two transitions in the total bandwidth are likely to occur, namely the transition from full bandwidth B_F, to B_I $(0<B_I<B_F)$, and finally to zero bandwidth. Unfortunately, there are no rigorous results concerning the nature of the spectrum for any Penrose lattices, and so apart from the analytical results concerning a few select eigenstates of a Penrose lattice composed of rhombs,[32,33] our understanding of the spectral properties of these structures is limited to conjectures based on numerical data for finite-size rhombus-based lattices.[23–29]

Another feature of one-dimensional quasiperiodic systems which has received considerable attention concerns the existence of a so-called gap-labeling theorem[34,35] which allows us to label spectral gaps by the integrated density of states. To be precise, for the case of the Fibonacci-chain quasicrystal, the integrated density of states corresponding to an energy (or frequency) in a spectral gap is given by $\{m\tau\}$, where m is a positive or negative integer, and $\tau=\frac{1}{2}(1+\sqrt{5})$ is the golden mean. Furthermore, the largest gaps correspond to the smallest integer values. To the best of our knowledge, the possibility that such a gap-labeling theorem also exists for higher-dimensional quasiperiodic lattices, including the Penrose lattice, has not been considered.

The organization of this paper is as follows: Section II is devoted exclusively to those properties of two-dimensional quasicrystals which depend only on the spectrum and includes analyses of the total bandwidth as well as the density and integrated density of states. For the higher-dimensional Fibonacci systems (Sec. II A), an exact convolution technique is developed which provides relationships to the corresponding dynamical properties of the Fibonacci chain for which the exact decimation technique, outlined in Appendix A, can be used. We present results for the density and integrated density of states for both the Fibonacci quasilattice and superlattice, and discuss the extent to which a gap-labeling theorem is applicable. Our study of the total bandwidth of these two-dimensional extensions again relies on the convolution identity, enabling us to obtain the two-dimensional bandwidth from that of the one-dimensional counterparts. Following Kohmoto[9] we consider periodically repeated Fibonacci chains and their extension to two dimensions, for which the notion of bandwidth is well defined. One of the qualitatively new features seen in the spectrum of the two-dimensional Fibonacci quasilattice is the appearance of two transitions: as a ratio of coupling strengths changes through some critical value, the number of bands (or gaps) changes from finite to infinite. At a second critical ratio the total bandwidth changes from finite to zero. Neither of these transitions is present in one dimension. A "simple," but nevertheless not completely solved, model (convolution of two Cantor sets) which illustrates how two such transitions can occur, is given in Appendix B.

In Sec. II B we present our results for the two-dimensional Penrose lattice composed of Robinson tiles. Unlike the higher-dimensional analogues of the Fibonacci chain, no exact convolution statement exists for the Penrose lattice due to its complicated geometry. Consequently our results are based on the direct diagonalization of finite-size samples, yielding a collection of eigenvalues and their corresponding eigenvectors. Our analysis of the spectrum indicates that the gap number is always finite as is the total bandwidth. In addition, plots of the integrated density of states for both electron and phonon dynamics are given and a gap-labeling theorem is discussed.

Section III is concerned with the study of the full energy (or frequency) and wave-vector-dependent response function $S(\mathbf{q},E)$ for the same two-dimensional quasicrystals studied in Sec. II. The convolution identity for the two-dimensional density and integrated density of states developed in Sec. II is extended to the investigation of the dynamic-structure factor (Sec. III A) allowing us to express $S(\mathbf{q},E)$ for the two-dimensional Fibonacci systems as exact convolutions of one-dimensional dynamic-structure factors, which can be obtained using the decimation method.[16] Furthermore, by extending an analysis for the one-dimensional case, an exact expression is obtained for the dynamic-response function for the two-dimensional Fibonacci quasilattice in the limit of equal couplings, whose support is an infinite family of "dispersion" curves. For unequal couplings these curves lose their identity, developing a dense set of gaps at their crossing points, and this allows both an interpretation of gap-labeling rules identifiable in the integrated density of states and of the computed surface plots for the response function. Rather different features are seen in the computed response function for the Penrose lattice, where no "equal-coupling" case is ever appropriate, due to the intrinsic difficulty associated with the geometry.

II. SPECTRUM AND DENSITY OF STATES

Since rather different techniques are required for the two-dimensional Fibonacci lattices and for the Penrose lattice, we discuss these separately in the two subsections which now follow.

A. Two-dimensional Fibonacci lattices: Convolution and decimation

The models we have considered are direct extensions to higher dimensions of the Fibonacci chain. This exists in both bond and site versions, which can be related. In the bond version, it is a chain of atoms linked by two types of nearest-neighbor bonds, A or B, in a Fibonacci sequence, which can be obtained by projection or by using the recursive process $A\rightarrow AB, B\rightarrow A$ to construct a sequence

of generations. Both electron and phonon dynamics can be discussed: to maintain generality we will talk in terms of the tight-binding electronic case, which includes phonons or spin waves as special cases, the latter two containing a Goldstone symmetry.

Let $\mathbf{H}_A$ and $\mathbf{H}_B$ denote two one-dimensional Hamiltonians of the tight-binding form, with corresponding eigenvalues $\{E_\alpha\}$ and $\{E_\beta\}$ and eigenstates $\{|\alpha\rangle\}$ and $\{|\beta\rangle\}$, respectively. Then, provided the potential of the two-dimensional system is separable, the Hamiltonian of the composite system is given by

$$\mathbf{H}=\mathbf{H}_{A,x}\otimes\mathbf{I}_y+\mathbf{I}_x\otimes\mathbf{H}_{B,y} , \tag{2.1}$$

where $\mathbf{I}_x$ and $\mathbf{I}_y$ denote the identity operators acting in the x and y subspaces, respectively, and the eigenvalues and eigenstates of the composite system are

$$E_{\alpha\beta}=E_\alpha+E_\beta , \tag{2.2a}$$

$$|\alpha\beta\rangle=|\alpha\rangle\otimes|\beta\rangle . \tag{2.2b}$$

Now, the density of states of the two-dimensional composite system is, by definition, given by

$$\rho(E)=\sum_{\alpha\beta}\delta(E-E_{\alpha\beta}) =\sum_\alpha \rho_B(E-E_\alpha) . \tag{2.3}$$

Then inserting a δ function into (2.3) and performing the sum over α, allows us to write

$$\rho(E)=\int dE'\rho_A(E')\rho_B(E-E') , \tag{2.4}$$

which expresses the two-dimensional density of states as a convolution of the densities of states ρ_A and ρ_B of the one-dimensional Hamiltonians $\mathbf{H}_A$ and $\mathbf{H}_B$. A similar result has been obtained independently by Schwalm and Schwalm.[22] Furthermore, it follows by straightforward integration that

$$N(E)=\int dE'\rho_A(E')N_B(E-E') \tag{2.5}$$

is the corresponding result for the two-dimensional integrated density of states. The generalization of (2.4) to three dimensions is straightforward and yields the result

$$\rho(E)=\int\int dE'dE''\rho_A(E')\rho_B(E'')\rho_C(E-E'-E'') . \tag{2.6}$$

A special case of Eqs. (2.4) and (2.5) arises when $\mathbf{H}_A=\mathbf{H}_B$, corresponding to the convolution of densities of states associated with two identical Hamiltonians. The results presented in this chapter for the Fibonacci quasilattice will be for precisely this isotropic situation. The more general anisotropic case where $\mathbf{H}_A\neq\mathbf{H}_B$ corresponding to two Fibonacci-chain Hamiltonians characterized by different parameters, is not expected to display any new features. The case of the Fibonacci superlattice is, however, intrinsically anisotropic, necessitating the convolution of the densities ρ_F and ρ_P of the one-dimensional Fibonacci-chain Hamiltonian $\mathbf{H}_F$ and one-dimensional periodic Hamiltonian $\mathbf{H}_P$, respectively.

In what follows we shall consider systems whose dynamics is governed by Hamiltonians composed of those giving rise to the following three one-dimensional linear equations of motion:

$$(E-V_n)\psi_n=\psi_{n-1}+\psi_{n+1} , \tag{2.7a}$$

$$(E-\epsilon_n)u_n=\sum_m W_{nm}u_m , \tag{2.7b}$$

$$\left[\sum_m K_{mn}-\omega^2\right]\phi_n=\sum_m K_{nm}\phi_m . \tag{2.7c}$$

In (2.7a) V_n denotes a site-dependent potential, and ψ_n the wave function at site n. Equation (2.7b) is the usual tight-binding equation describing a single band, and ϵ_n and W_{nm} denote, respectively, the on-site energies and nearest-neighbor hopping-matrix elements. Equation (2.7c) describes harmonic excitations (scalar phonons), ϕ_n denoting the displacement at site n, and K_{nm} the spring constant joining sites n and m. If we interpret the force constants K_{nm} as exchange constants J_{nm} and replace the spectral variable ω^2 by ω, then (2.7c) describes the dynamics of Heisenberg ferromagnetic spin waves at zero temperature. The two-dimensional generalizations of these models are then as implied by (2.1).

Figures 1 and 2 show the resulting density of states (DOS) for electron and phonon dynamics as described by (2.7b) and (2.7c), respectively, on the two-dimensional Fibonacci quasilattice and Fibonacci superlattice obtained using the convolution formula (2.4). The symmetry under $E\leftrightarrow -E$ in the first case arises from having only hopping terms ($\epsilon_n=0$) in the Hamiltonian H_F. In the case of phonons (or spin waves) there is obviously no such symmetry. Moreover, the local scaling properties in this case are nonuniform because the invariant of the trace map for the one-dimensional case involves ω^2 explicitly. Results are given in Figs. 3 and 4 for the phonon and electronic integrated densities of states (IDOS) on the two-dimensional Fibonacci quasilattice, which appear to have a Devil's staircase structure. In addition, the linear behavior for small frequencies in the phonon problem implies the validity of a continuum viewpoint in this region.

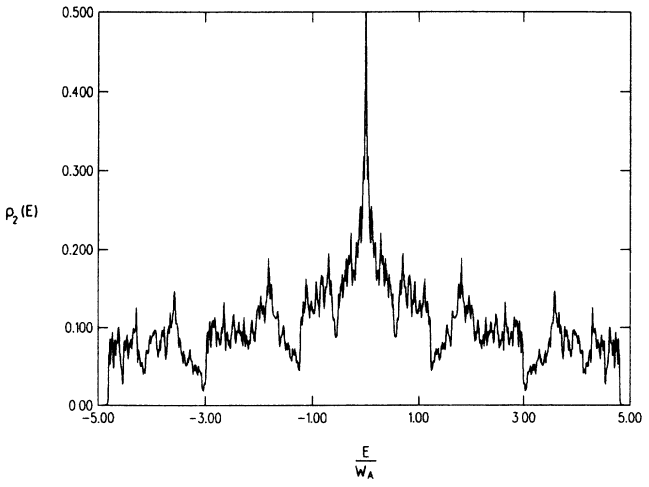

FIG. 1. The electronic density of states for the isotropic 2D Fibonacci quasilattice for $W_A=1$ and $W_B=1.5$.

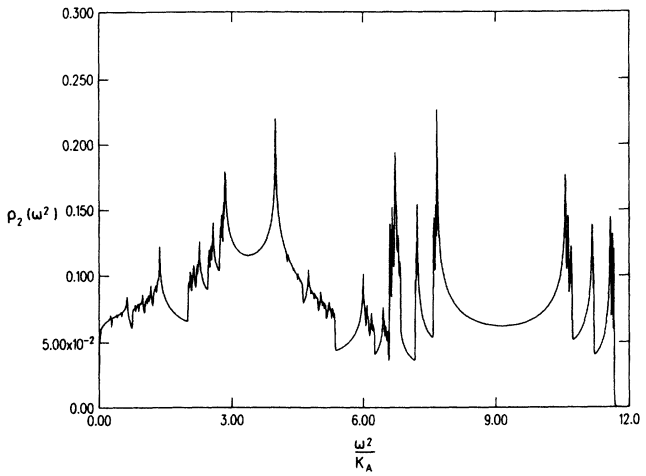

FIG. 2. The phonon density of states for the 2D Fibonacci superlattice for $K_p = K_A = 1$ and $K_B = 2.5$.

Indeed, such low-frequency behavior is expected to occur for any two-dimensional lattice having Goldstone dynamics, and indeed we shall see that it also occurs for the two-dimensional Penrose lattice. The plateaus in the integrated density of states for the electron and phonon cases, Figs. 3 and 4, occur at ordinate values which we have found to be of the form

$$H = \{m\tau\} , \tag{2.8}$$

where $\{\}$ denotes the "fractional part of," and m is a positive or negative integer. The values of m corresponding to a few of the largest gaps are indicated explicitly on these two figures. This allows the gaps to be labeled by the integer m, just as in one dimension. However, for the one-dimensional Fibonacci chain the largest gaps correspond to the smallest integer values in (2.8), whereas in two (and presumably higher) dimensions this is no longer the case. The gap-labeling result (2.8) is a generalization of that observed for the Fibonacci chain,[11] and its appearance in the two-dimensional Fibonacci system is explained in Sec. III A, using a perturbative argument starting from an exact result for the dynamic response function of two-dimensional Fibonacci lattices. Gap-labeling formulas are a very general property of quasiperiodic models.[34,35]

We shall now turn our attention to the more fundamental issues regarding the nature of the spectra of models described by (2.7), and, in particular, questions related to the total bandwidth and total number of gaps. In one dimension it is known that the energy or frequency spectra of models described by (2.7) have zero total bandwidth[31] and infinitely many gaps. We cannot always expect this in higher dimensions: for example, for the Fibonacci superlattice the total bandwidth B_S and band number N_S must always be finite, since under convolution the finite bandwidth $4W_p$ of the periodic spectrum E_k ($E_k = \varepsilon + 2W_p \cos k$) fills any gaps less than $2W_p$ in the Fibonacci-chain spectrum. Such considerations raise questions about possible transitions in total bandwidth B_{2F} and band number N_{2F} for other two-dimensional quasiperiodic models. To be specific we shall consider the two-dimensional version of the model whose dynamics is described by (2.7a) where the on-site potential V_n takes two values V_A and V_B according to the Fibonacci sequence, together with the condition $V_A = -V_B$. Furthermore, we shall assume that the underlying geometry is that of the two-dimensional Fibonacci quasilattice with isotropic, and later anisotropic, interactions.

A convenient formalism with which to study the energy spectrum of the one-dimensional Fibonacci chain is that based on the transfer matrix, introduced independently by Kohmoto, Kadanoff, and Tang[9] and by Ostlund and Pandit.[10] This approach uses the rule $A \to AB, B \to A$ to produce the following third-order difference equation for $\gamma_L = \frac{1}{2}\mathrm{Tr}(\mathbf{T}_L)$, where $\mathbf{T}_L$ is the transfer matrix describing level L of the hierarchy:

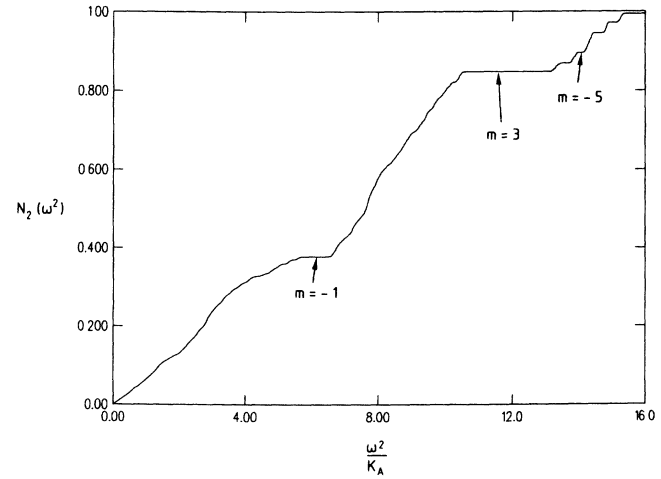

FIG. 3. The phonon integrated density of states for the isotropic 2D Fibonacci quasilattice for $K_A = 1$ and $K_B = 3$.

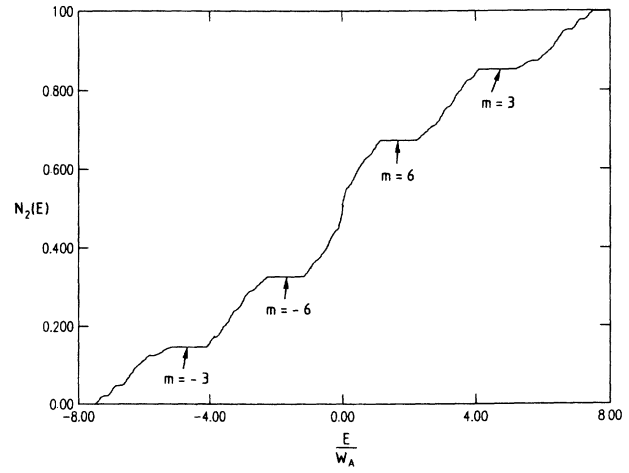

FIG. 4. The electronic integrated density of states for the isotropic 2D Fibonacci quasilattice for $W_A = 1$ and $W_B = 3$.

$$\gamma_{L+1}=2\gamma_L\gamma_{L-1}-\gamma_{L-2}\ . \tag{2.9}$$

γ_L is found by iterating (2.9) from three initial values, which for the case of (2.7a) are given by $\gamma_{-1}=1$, $\gamma_0=\frac{1}{2}(E-V_B)$, and $\gamma_1=\frac{1}{2}(E-V_A)$. If we imagine our Fibonacci chain at level L to be periodically repeated, then for such an (infinite) chain whose basic unit cell contains F_L sites, we expect the energy spectrum to consist of F_L bands ($F_L=F_{L-1}+F_{L-2}$, with $F_0=1$, $F_1=1$). The band edges $[a_i^{(L)},b_i^{(L)}]$ of such a system are obtained by solving the polynomial equation $\gamma_L=\pm 1$ of degree F_L. The band edges of the two-dimensional extension are then, by Eq. (2.4), simply obtained by forming $[a_i^{(L)}+a_j^{(L)},b_i^{(L)}+b_j^{(L)}]$ for all possible i and j from 1 to F_L. The union of all these bands yields the spectral support.

We have calculated the total bandwidth B_{2F} and band number N_{2F} for the two-dimensional Fibonacci quasilattice as functions of $V=V_A=-V_B$ for several system sizes. Figure 5 is a plot of the total bandwidth $B_{2F}^{(L)}$ versus V for $L=3,\ldots,11$, where L labels the order of iteration of the trace map (2.9) [so F_L is the length of the Fibonacci chain used in the composition (2.1)]. The extrapolation to $L\to\infty$ in the finite-size extrapolation plot in Fig. 6 provides strong evidence that the total bandwidth vanishes for $V>V_2$ where $V_2=1.95\pm0.05$. A finite-size analysis of the band number is given in Figs. 7 and 8 in which, respectively, $\ln N_{2F}^{(L)}$ and $N_{2F}^{(L)}/N_{2F}^{(L-2)}$ are plotted versus V for various values of L, where $N_{2F}^{(L)}$ is the band number at generation L. In the second plot (Fig. 8), L and $L-2$ are used to reduce alternation effects from the recursive construction. The asymptotic value of $N_{2F}^{(L)}/N_{2F}^{(L-2)}$ at large V becomes τ^4, because in that regime the bands become very small, and hence their number in a two-dimensional system of side length F_L is proportional to F_L^2, i.e., to τ^{2L}, for large L, where $\tau=\frac{1}{2}(1+\sqrt{5})$ is the golden mean. At weak coupling a

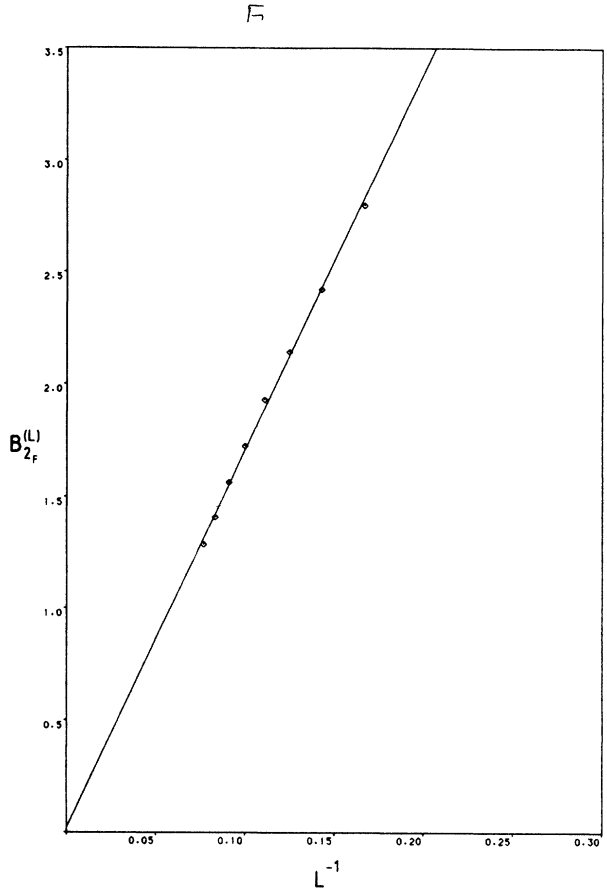

FIG. 6. The finite-size extrapolation of the total bandwidth $B_{2F}^{(L)}$ of the isotropic 2D Fibonacci quasilattice for $V=1.9$ and $L=6,7,\ldots,13$.

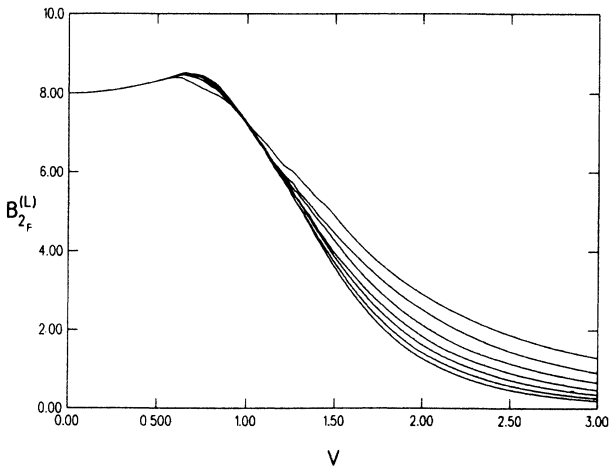

FIG. 5. The total bandwidth $B_{2F}^{(L)}$ as a function of $V=V_A=-V_B$ for the isotropic 2D Fibonacci quasilattice with $L=5,6,\ldots,11$.

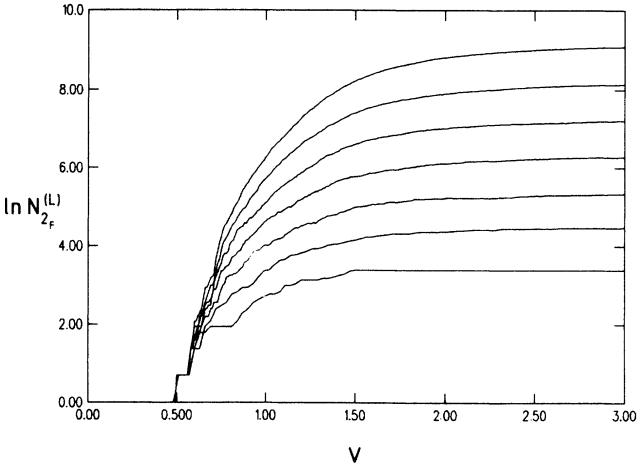

FIG. 7. The logarithm of the total number of bands $N_{2F}^{(L)}$ as a function of $V=V_A=-V_B$ for the isotropic 2D Fibonacci quasilattice with $L=5,6,\ldots,11$.

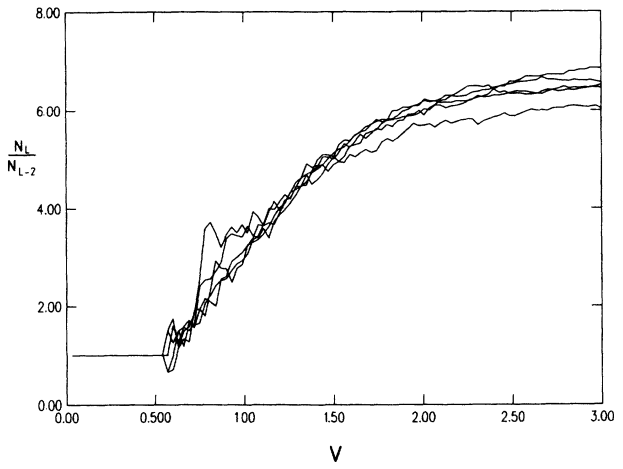

FIG. 8. $N_{2F}^{(L)}/N_{2F}^{(L-2)}$ as a function of $V=V_A=-V_B$ for isotropic Fibonacci square lattice for $L=7,8,\ldots,11$.

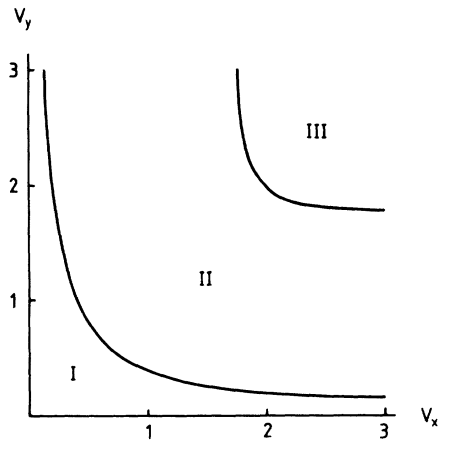

FIG. 10. The phase diagram for the anisotropic Fibonacci square lattice.

single band is apparent in the figures. There is a small domain around $V=0.5$ where two bands can be identifiable. The two figures clearly show a transition from finite to infinite band number at $V=V_1\approx 0.6$. The question of whether there are higher finite numbers of bands in a narrow region below V_1 is not clear. The resulting "phase diagram" for the case of electron dynamics on the two-dimensional Fibonacci quasilattice is shown in Fig. 9. The region I ($V<V_1$) is where band number N_{2F} and total bandwidth B_{2F} are both finite; region II ($V_1<V<V_2$) is where B_{2F} remains finite, but the transition to infinite N_{2F} has occurred; in region III ($V>V_2$) the second transition, to zero bandwidth, has occurred, and so $B_{2F}=0$ while N_{2F} is infinite. It is worth commenting that our results are consistent with those of Ueda and Tsunetsugu[21] who have investigated a particular anisotropic model with an equation of motion given by (2.7a) but found only the single transition to zero bandwidth.

These two transitions can be illustrated in a simple model involving convolution of two Cantor sets, each formed by the usual hierarchical process of subdividing, with a central gap, each subband of the previous generation. The convolution is described in Appendix B, first for a symmetric subdivision, where both transitions occur together, and then for the much more difficult case of an asymmetric subdivision, where the transitions occur at different parameter values. A general solution of this model has eluded us.

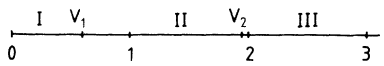

FIG. 9. The phase diagram for isotropic Fibonacci square lattice.

An interesting question is how the phase diagram of Fig. 9 generalizes for the anisotropic 2D Fibonacci quasilattice with different potentials V_x, V_y in the two directions. From the result for the case $V_x=V_y$, we know that three regions (corresponding to I, II, and III in Fig. 9) must occur in the V_x, V_y phase plane. Whether region II is of finite or infinite extent is not, however, decided by the isotropic case. The extension of our analysis to the anisotropic case for specific values of V_x, V_y using an obvious generalization of (2.3), yields points on the phase boundaries, as shown in Fig. 10. While these have provided some further details of the phase diagram, we are unable to say whether or not region II is bounded. Figure 10 incorporates some information about the phase boundaries obtained by considering the limits $V_x\to 0$ or $V_y\to\infty$ (and similarly with $V_x\leftrightarrow V_y$); these are uncoupled Fibonacci chains or Fibonacci chains periodically extended into the second dimension, which are in phases III or I, respectively, and imply that both these boundaries approach the axes.

B. Penrose lattice: Construction and spectral properties

Penrose lattices can be generated either by projection[36,37] (i.e., from five to two dimensions), by the generalized dual method,[38] or multigrid method,[29] producing tilings composed of two types of rhombs, or by a deflation approach applied to darts and kites.[40] An alternate method is the recursive construction of Robinson[4,18,19] based on the successive subdivisions of two triangular tiles (Robinson tiles), according to the following rules:

$$P\to 2P+Q\ , \tag{2.10a}$$

$$Q\to P+Q\ , \tag{2.10b}$$

where P and Q denote the two basic triangles whose angles are $(\pi/5,2\pi/5,2\pi/5)$ and $(3\pi/5,\pi/5,\pi/5)$, respectively. It is also worth mentioning that, in addition to the basic inflation rules (2.10), it is also necessary to impose matching rules by associating a chirality with each of the P and Q tiles. After n iterations of the recursion relations (2.10) starting from a P triangle, we arrive at a tiling containing F_{2n} P-type triangles and F_{2n-1} Q-type triangles, where F_n is again the nth Fibonacci number. In Fig. 11 we illustrate a finite Penrose lattice containing 217 vertices, obtained after six iterations of (2.10) starting from a P-type triangle. By cutting the darts and kites of a Penrose tiling obtained by projection one obtains the two triangles of the Robinson construction, and so clearly a tiling composed of Robinson triangles is more highly connected than one obtained by projection, and this difference shows up in the excitation spectra of the systems we have studied on these geometries.

The sites of the resulting finite lattices do not, of course, lie on a regular lattice, unlike the two-dimensional Fibonacci lattices just discussed, and so no convolution relationship of type (2.4) to a lower dimensional system is possible. Instead it is necessary to diagonalize a dynamical (or Hamiltonian) matrix, characterized by nearest-neighbor spring constants K_L and K_S (or hopping matrix elements W_L and W_S) between sites separated by a long and a short bond, respectively.

It is important to note that each iteration of (2.10) does not always produce new vertices, and so to ensure that each vertex is enumerated only once, it is necessary to calculate the coordinates (x_n,y_n) of every vertex n at each stage. For the case of electron dynamics, the diagonal elements (i,i) of the Hamiltonian matrix (i.e., the on-site energies) are taken to be zero for convenience, the off-diagonal elements (i.e., the nearest-neighbor hopping-matrix elements) taking one of two values, W_L or W_S, according to the bond length. For the case of phonon dynamics the diagonal elements of the dynamical matrix cannot be zero because the Goldstone symmetry must be respected. Indeed, it is most convenient to use the Goldstone symmetry to generate the diagonal terms from the off-diagonal terms using the fact that the sum of all entries in any row or column of the dynamical matrix must be identically zero.

The resulting integrated density of states $N_P(E)$ for electron dynamics and $N_P(\omega^2)$ for phonon dynamics on the Penrose lattice containing 2191 vertices is shown in Figs. 12 and 13. Figure 13 shows several clearly resolved gaps, however, these appear to be fewer in number than found for the corresponding spectra for Penrose lattices composed of darts and kites[24] or rhombs.[23,26] In addition, in the low frequency or continuum limit the phonon IDOS clearly displays a linear behavior characterized by the same exponent, namely $d/2$, as occurs in regular lattices of the same dimension. For both the phonon and electron cases, the integrated density of states shows a gap-labeling feature, the plateaux occurring at ordinate values which are again given by (2.8). The values of m associated with a particular gap are indicated on the figures.

The possibility that the Penrose lattice has the same two transitions seen in the 2D Fibonacci system is considered next. Since the numerical technique produces only discrete states, rather than bands, the method of analysis used previously cannot be applied to the Penrose lattice results. Instead, a finite-size analysis is performed on the total number of gaps $H^{(L)}(\Delta)$ whose size is greater than Δ. Figure 14 is a plot of $H^{(L)}(\Delta)$ versus Δ for the

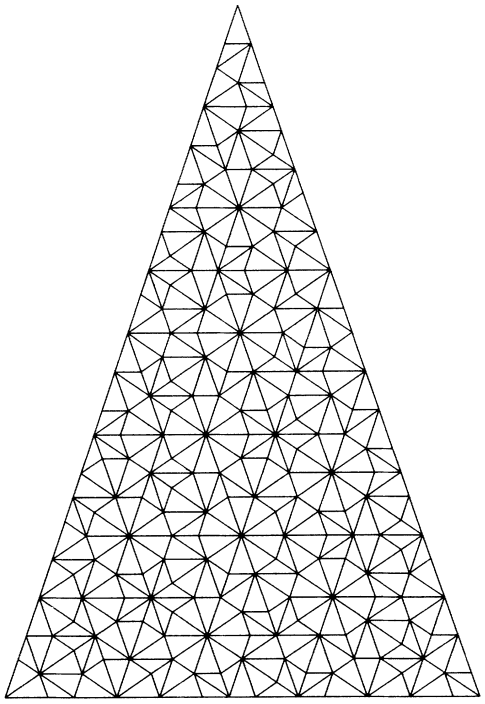

FIG. 11. A finite portion of a Penrose lattice containing 217 sites obtained from a P triangle after six iterations.

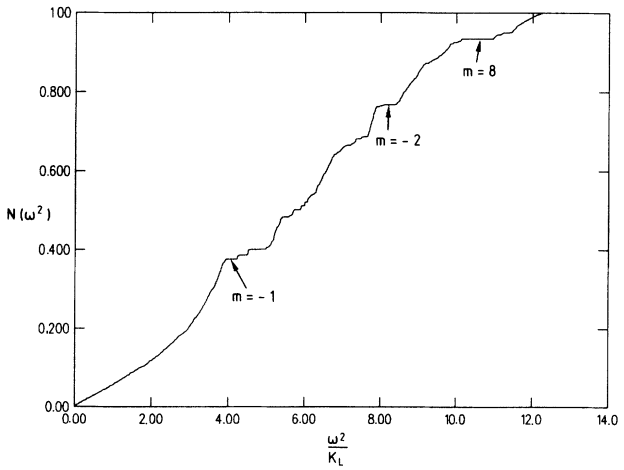

FIG. 12. The integrated phonon density of states for a 2D Penrose lattice composed of Robinson tiles, consisting of 2191 sites, for $K_A=K_B=1$.

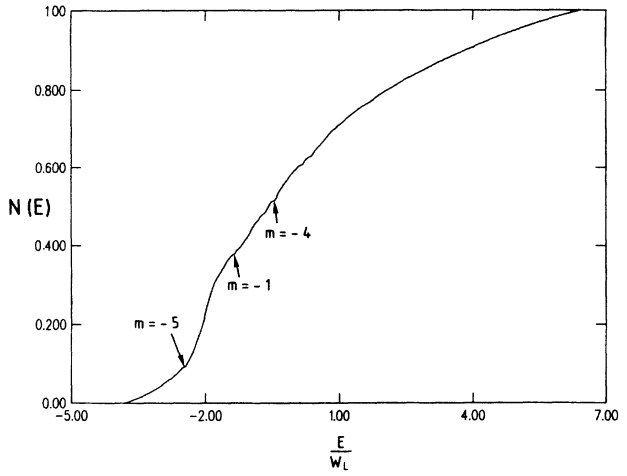

FIG. 13. The integrated electron density of states for a 2D Penrose lattice composed of Robinson tiles, consisting of 2191 sites, for $W_A = W_B = 1$.

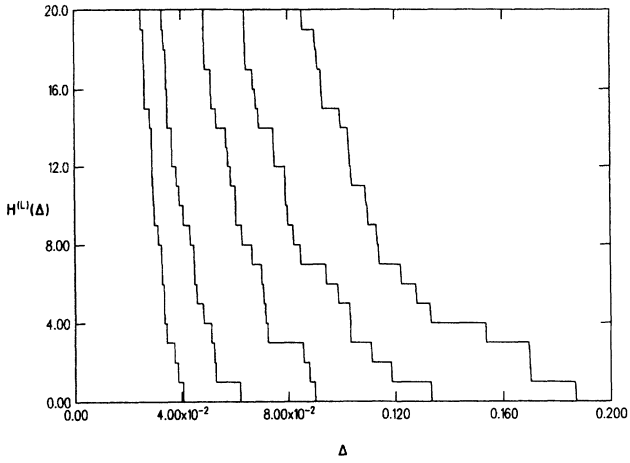

FIG. 14. $H^L(\Delta)$ vs Δ for electrons with $W_L = W_S = 1$.

case of equal-coupling electrons for different values of L, where L is now the generation number of the Penrose lattice, i.e., the number of times the recursive tiling technique has been iterated starting from either a P or a Q triangle. The values of L we have used correspond to systems containing 344, 539, 861, 1365, and 2191 lattice sites. The data suggests that $H^{(L)}(\Delta)$ is a decreasing function of L, for large enough L, and any fixed $\Delta \neq 0$ and that the gap number is always finite. This statement appears to be universal (independent of system parameters), and so the transitions between finite and infinite gap number and zero and nonzero bandwidth appear not to occur for the Penrose lattice.

Generic plots of the energy spectrum versus $W = W_S/W_L$ and $K = K_S/K_L$ have been obtained (Figs. 15–17) which exhibit the following additional features: In the phonon system gaps become small at small ω because of the asymptotic validity of the continuum view described above. In the high-frequency regime of the two figures, ω^2 and E are becoming linear in W or K at large W or K: this is because in this limit only the stronger of the two bonds matters. A similar argument using the dominance of the unit bonds as $W \to 0$ explains the W independence of the electronic spectrum at small W. In the phonon case, however, the "Goldstone symmetry" makes the weak bonds equally important for the low-frequency behavior and that is indeed seen to depend strongly on K at small K.

III. DYNAMIC RESPONSE FUNCTION

The dynamic-structure factor or response function $S(\mathbf{q},E)$ is the linear response of the system to a dynamic probe (coupling linearly to the dynamical variable) at energy E and wave vector $\mathbf{q}$. Its $\mathbf{q}$ integral or E integral give, respectively, the density of states $\rho(E)$, or the static structure factor $S(\mathbf{q})$ which is measured in diffraction experiments. In simple systems $S(\mathbf{q},E)$ is sharply peaked where E and $\mathbf{q}$ satisfy "dispersion relationships" of the form $E = f(\mathbf{q})$, describing the excitation energies of the eigenmodes. It will be seen in the following subsections that a generalization of this statement to many dispersion curves provides an accurate description of the dynamic response of the two-dimensional Fibonacci quasicrystals, for certain regimes of couplings, while the Penrose lattice response is never of a simple form.

A. Two-dimensional Fibonacci systems; Convolution method for response

The response functions of the periodically and quasiperiodically extended Fibonacci lattices both satisfy convolution statements which arise, as in Sec. II A, from the separability property of the potential. As before, let $|\alpha\rangle$ and $|\beta\rangle$ denote the eigenstates of the one-dimensional Hamiltonians $\mathbf{H}_A$ and $\mathbf{H}_B$, corresponding to the eigenvalues E_α and E_β, respectively. Then, by definition, the response function of the two-dimensional extension is given by

$$S(\mathbf{q},E) = \sum_{\alpha\beta} \int dx\,dx'\,dy\,dy'\,e^{i\mathbf{q}\cdot(\mathbf{r}-\mathbf{r}')} \langle xy|\alpha\beta\rangle \times \delta(E - E_{\alpha\beta}) \langle \alpha\beta|x'y'\rangle \,, \tag{3.1}$$

where $\mathbf{q} = (q_x, q_y)$ and $\mathbf{r} = (x,y)$. Then, rewriting $\delta(E - E_{\alpha\beta})$ in the form

$$\int dE' \delta(E' - E_\alpha) \delta(E - E' - E_\beta) \,,$$

and using the fact that $\langle xy|\alpha\beta\rangle \equiv \langle x|\alpha\rangle \langle y|\beta\rangle$, it follows that

$$S(\mathbf{q},E) = \int dE' S_A(q_x,E') S_B(q_y, E - E') \,, \tag{3.2}$$

where S_A and S_B denote the dynamic-structure factors of the one-dimensional Hamiltonians $\mathbf{H}_A$ and $\mathbf{H}_B$, respec-

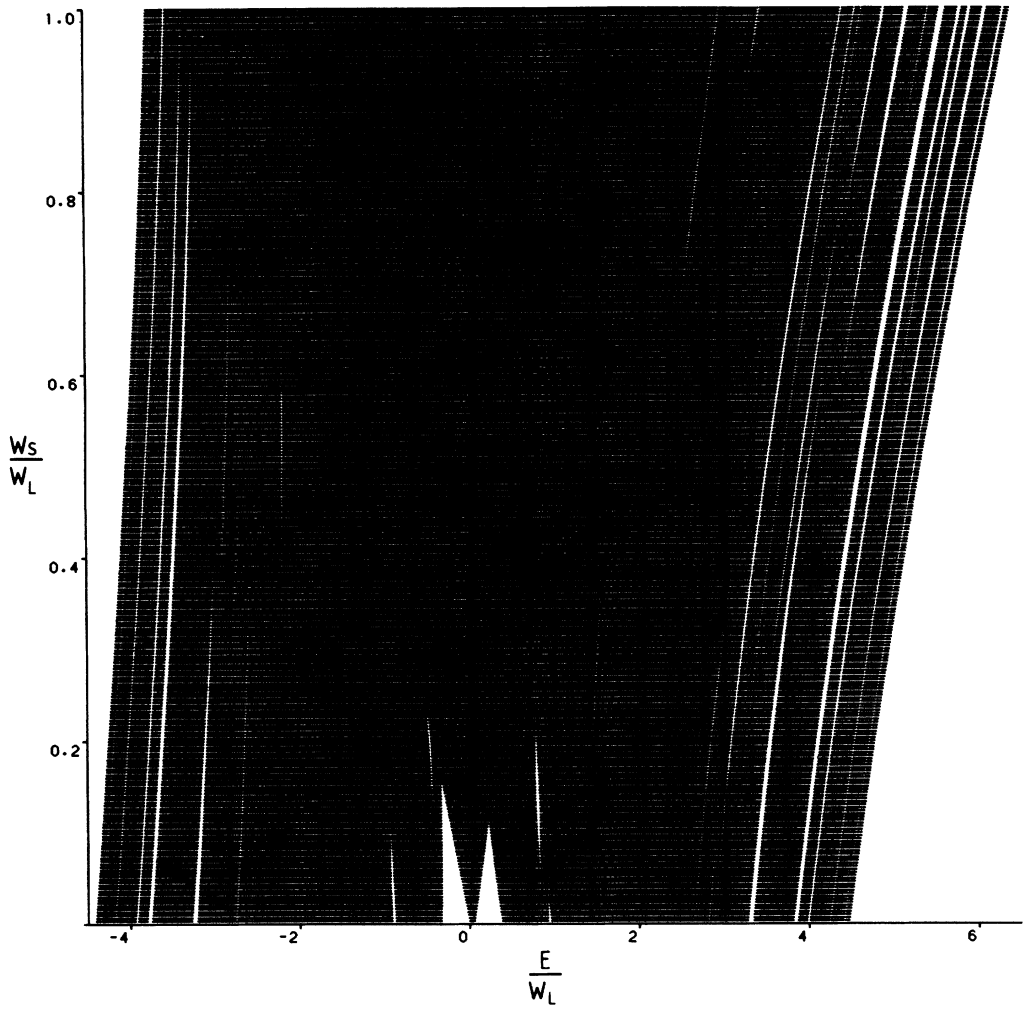

FIG. 15. The energy spectrum for a 2D Penrose lattice composed of Robinson tiles, consisting of 539 sites ($0 \leq W \leq 1$).

tively, and it is implicitly assumed that a finite imaginary part has been added to the spectral variable E in order to regularize the functions. Generalizations to three dimensions follow in exactly the same way as in Sec. II for the density of states.

According to (3.2), the dynamic-structure factor for the Fibonacci superlattice is equal to the convolution of the one-dimensional Fibonacci-chain dynamic-structure factor $S_F(q_x,E)$ with that of the one-dimensional uniform chain $S_P(q_y,E)=\delta(E-E_{q_y})$, where $E_{q_y}=\epsilon+2W\cos q_y$. It is thus possible to perform the integral in (3.2) leading to the result

$$S(\mathbf{q},E)=S_F(q_x,E-E_{q_y}) \tag{3.3}$$

for the dynamic-structure factor for the two-dimensional Fibonacci superlattice. Furthermore, a simple extension of this to three dimensions leads to

$$S(\mathbf{q},E)=S_F(q_x,E-E_{q_y}-E_{q_z}) . \tag{3.4}$$

These results illustrate that the dynamic-structure factors of the two- and three-dimensional Fibonacci superlattices are determined solely by that of the one-dimensional Fibonacci chain, studied in detail in Ref. 16. Figure 18 shows the resulting structure factor $S_{FF}(\mathbf{q},E)$ for electron dynamics on the 2D Fibonacci quasilattice as a surface plot, S_{FF} versus $|\mathbf{q}|$ and E for $\mathbf{q}$ in the (1,1) direction. Figure 19 is the corresponding result for phonon dynamics, namely $S(\mathbf{q},\omega^2)$, again with $\mathbf{q}$ along the (1,1) direction. All the figures show sharp structure suggesting definite ridges and valleys, very like results obtained previously for the Fibonacci-chain response function S_F. In particular, results for $S_{FF}(\mathbf{q},\omega^2)$ with $\mathbf{q}=(q,0)$ (not shown) are identical with those obtained previously[16] for $S_F(q,\omega^2)$; this is explained by using in (3.2) the result $S_F(q_y,\omega^2-\omega'^2)\sim\delta(\omega^2-\omega'^2)$ for small q_y. The sharp peaking in $S_F(q,\omega^2)$ at small q is inherited [via (3.2)] by the two-dimensional response functions.

To see this peaking more clearly, and to see the general structure of ridges and valleys, we have also plotted the

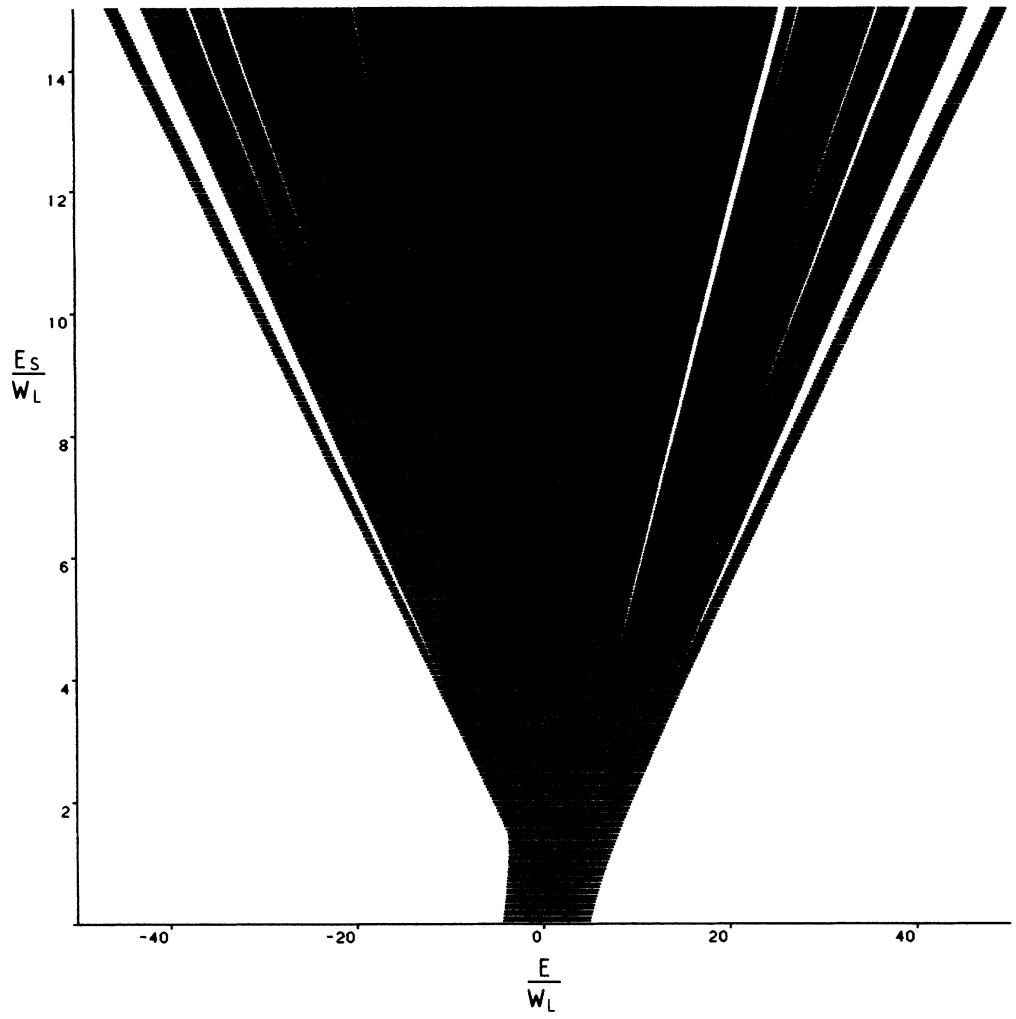

FIG. 16. The energy spectrum for a 2D Penrose lattice composed of Robinson tiles, consisting of 539 sites ($0 \leq W \leq 10$).

support of $S_{FF}(\mathbf{q},\omega^2)$, i.e., the regions in $(\mathbf{q},\omega^2)$ space where $S_{FF}(\mathbf{q},\omega^2)$ is appreciable. Figures 20 and 21 are the supports of $S_{FF}(\mathbf{q},\omega^2)$ for phonon dynamics in the 2D Fibonacci quasilattice with $\mathbf{q}=(q,q)$, for equal and unequal coupling ratios respectively. Dispersion curves of the sort seen earlier for the Fibonacci chain are obvious in the equal coupling plot, Fig. 20. In Fig. 21 the dispersion curves are again identifiable, but they have been modified by the opening up of gaps at their crossing points. As in the Fibonacci chain, these figures can be understood in terms of an exact result for the equal-coupling case and its perturbation theory extension. An outline of this description is now given, which also helps to explain the gap-labeling result (2.8).

For the equal-coupling case, the eigenenergies of the Fibonacci chain become those (E_k say) of a uniform chain and the eigenfunctions are of the form $\langle n|k\rangle = e^{ikn}$ if n is a site label, whose relationship to the coordinate x is

$$x_n = \alpha n - \frac{1}{\tau}\{n\tau\} , \tag{3.5}$$

where $\alpha = 1+1/\tau^2$. The coordinate x_n of the nth site still complicates the defining expression for $S_F(q,E)$ because of the Fourier transform involved. But the periodicity of the fractional part $\{\ \}$ can be used to reduce the transform,[16,41] with the result

$$S_F(q,E) = \sum_{m=-\infty}^{\infty} F_m(q)\delta(E - E_{\alpha q - 2\pi m\tau}) , \tag{3.6}$$

where

$$F_m(q) = [2(\sin q/2\tau)/(q/\tau - 2\pi m)]^2 .$$

Inserting into (3.2) yields, for the equal-coupling case,

$$S_{FF}(\mathbf{q},E) = \sum_{mm'} F_m(q_x)F_{m'}(q_y) \times \delta(E - E_{\alpha q_x - 2\pi m\tau} - E_{\alpha q_y - 2\pi m'\tau}) . \tag{3.7}$$

The result (3.7) involves a sum over branches (labeled by m,m') for each of which E follows the dispersion curves of a uniform square lattice (with displaced $\mathbf{q}$). Because of the $F_m(q)$ factors, the strongest response at small $\mathbf{q}$

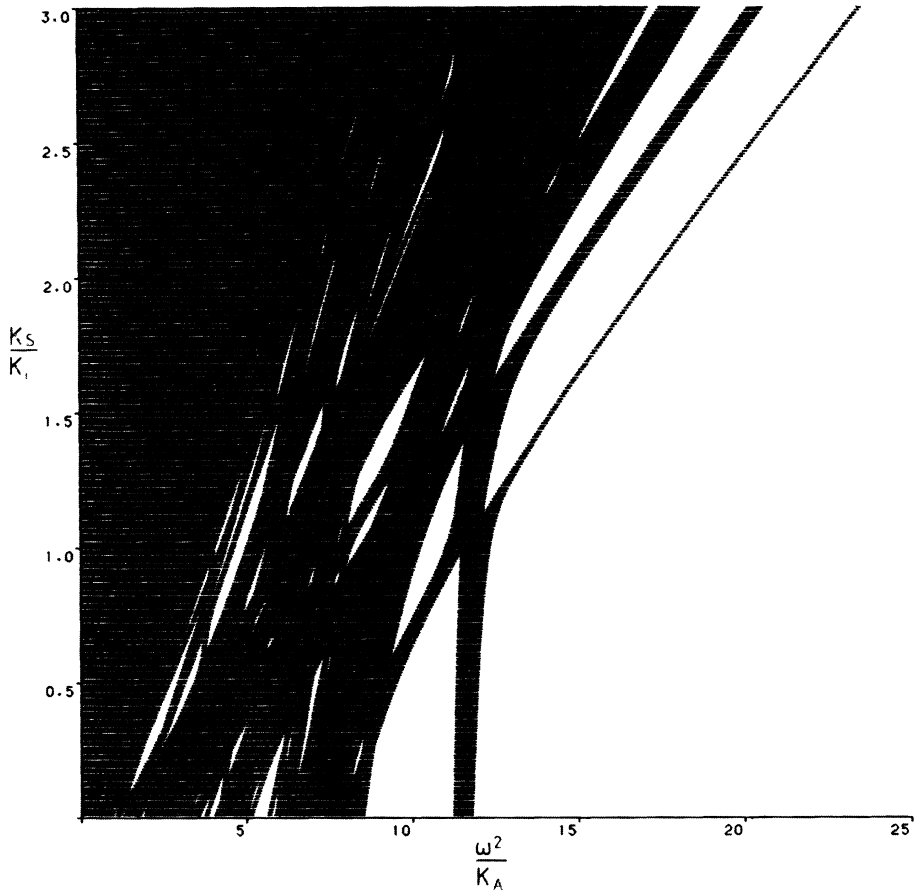

FIG. 17. The frequency spectrum for a 2D Penrose lattice composed of Robinson tiles, consisting of 539 sites ($0 \leq K \leq 3$).

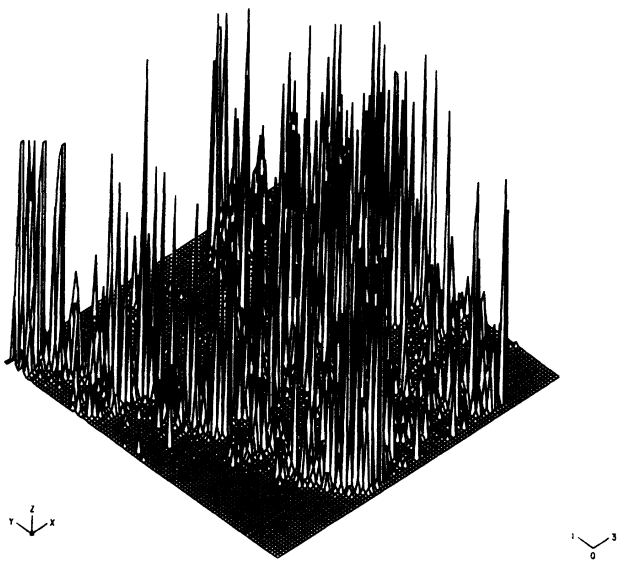

FIG. 18. A surface plot of $S(\mathbf{q},E)$ for electron dynamics on the isotropic Fibonacci square lattice for $\mathbf{q}$ in the (1,1) direction and $W_A=1$, $W_B=2$. The x axis corresponds to q for $0 \leq q \leq 2\pi$ and the y axis to E/W_A for $-6 \leq E/W_A \leq 6$.

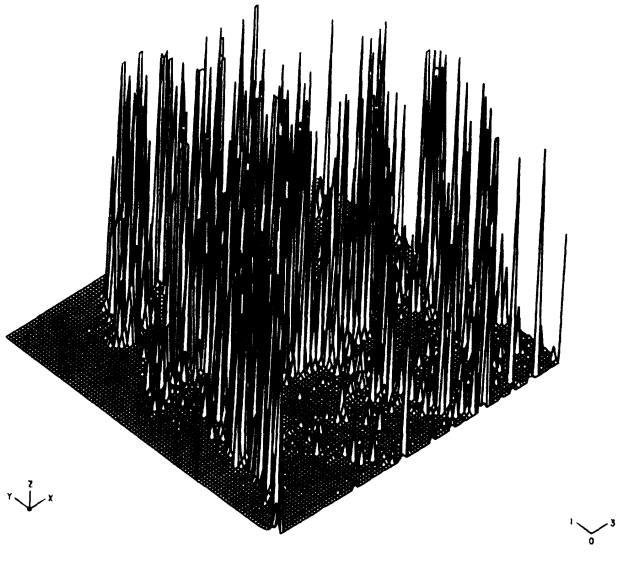

FIG. 19. A surface plot of $S(\mathbf{q},\omega^2)$ for phonon dynamics on the isotropic Fibonacci square lattice for $\mathbf{q}$ in the (1,1) direction and $K_A=1$, $K_B=2$. The x axis corresponds to q for $0 \leq q \leq 2\pi$ and the y axis to ω^2/K_A for $0 \leq \omega^2/K_A \leq 12$.

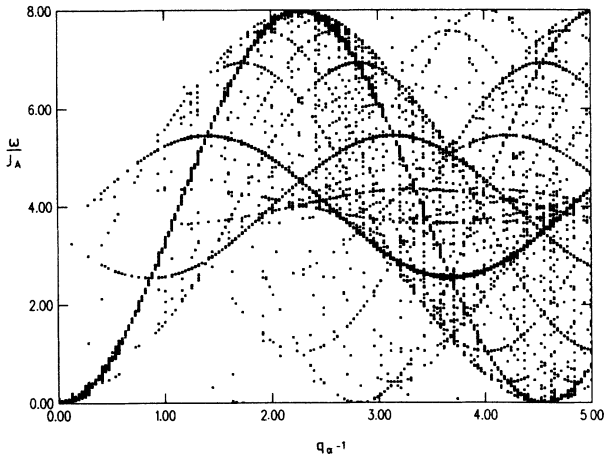

FIG. 20. A plot of ω^2 vs $\mathbf{q}$ for phonon dynamics on the isotropic 2D Fibonacci quasilattice for $\mathbf{q}$ along the (1,1) direction and $K_A=K_B=1$.

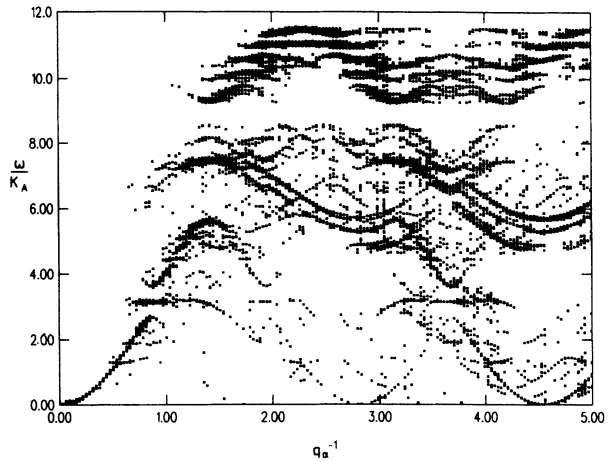

FIG. 21. A plot of ω^2 vs $\mathbf{q}$ for phonon dynamics on the isotropic 2D Fibonacci quasilattice for $\mathbf{q}$ along the (1,1) direction and $K_A=1$ and $K_B=2$.

comes from the $(m,m')=(0,0)$ branch, which is the effective-medium branch corresponding to the long-wavelength probe seeing the system as a square lattice with average spacing a (the weighted average of the A and B bond lengths). The result (3.7) provides a detailed explanation of Fig. 20.

To explain Fig. 21 it is necessary now to allow for the effect of unequal couplings. If the coupling difference is small, perturbation ideas can be used. These result in a coupling of the different branches, at their crossing points. The gaps that appear there are those seen in Fig. 21. Moreover, these gaps occur in $E_{\mathbf{k}}$ (or $\omega_{\mathbf{k}}$) at $\mathbf{k}=(k_x,k_y)$ where (in a reduced zone scheme) k_x and k_y are given in terms of positive or negative integers n_x,n_y by equations of the form

$$k_\alpha=\pi\{n_\alpha\tau\} \ . \tag{3.8}$$

These lines divide the $\mathbf{k}$-space reduced zone into an infinity of subzones. So, for weak coupling where $\mathbf{k}$ is both the wave vector and the mode counting label, plateaux in the (normalized) integrated density of states occur at values which are, apart from a factor $1/\pi^2$, sums of areas of neighboring subzones. This leads to (2.8) for the gap labeling and is valid to all orders in perturbation theory. The theory[42] also explains why the principal gaps are not associated with the smallest values of m in (2.8), as they would be for the Fibonacci chain at weak coupling, and why in general plateaux do not occur for all m.

B. Penrose lattice

Since no relationships to lower-dimensional subsystems apply for the Penrose lattice, its response function $S_P(\mathbf{q},\omega^2)$ for a phonon system, must be calculated from first principles. We have chosen to calculate $S_P(\mathbf{q},\omega^2)$ by computing the eigenvalues ω_α^2 and eigenvectors $|\alpha\rangle$ of the dynamical matrix and using the relation

$$S(\mathbf{q},\omega^2)=\sum_\alpha \delta(\omega^2-\omega_\alpha^2)|\langle \mathbf{q}|\alpha\rangle|^2 \ , \tag{3.9}$$

where, in practice, we replace the δ function by a normalized Lorentzian of width η. An alternative approach based on the equation of motion method of Alben *et al.*[43] has recently been employed by Patel and Sherrington[44] in their investigation of the propagating modes on a Penrose lattice obtained by projection.

The resulting surface plot of the Penrose lattice response function $S_P(\mathbf{q},\omega^2)$ is shown in Fig. 22 for phonon dynamics for the uniform coupling ratio $K_L=K_S=1$ and $\mathbf{q}=(q,q)$. The results are much less singular in appearance than those (Figs. 20 and 21) for the 2D Fibonacci quasilattice and there is little suggestion of anything analogous to a dispersion curve. This is because, for the Penrose lattice, there is no simplifying value of the cou-

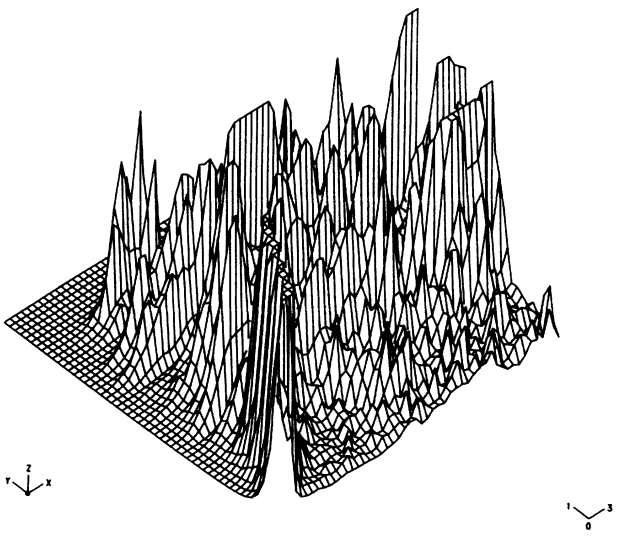

FIG. 22. A surface plot of $S(\mathbf{q},\omega^2)$ for phonon dynamics on a 2D Penrose lattice composed of Robinson tiles for $\mathbf{q}$ along the (1,1) direction and $K_L=K_S=1$. The x axis corresponds to q for $0\le q\le 10\pi$ and the y axis to ω^2 for $0\le\omega^2\le 12$.

pling ratio K, in contrast to the 2D Fibonacci quasilattice, where the case of equal couplings leads to the family of curves obvious in Fig. 20. Nevertheless, at small $|\mathbf{q}|$, the support is expected to be strongly peaked on an effective medium or continuum dispersion curve $\omega=c|\mathbf{q}|$ for the reason discussed earlier that at long wavelengths the excitation sees the Penrose lattice as an isotropic continuum (the structures with scales larger than wavelength $1/|\mathbf{q}|$ having vanishingly small weight in the limit of the wavelength going to infinity), provided localization effects do not play an overriding role. This expectation of a small $|\mathbf{q}|$ dispersion curve is supported by Fig. 22.

IV. DISCUSSION

This investigation has produced detailed results for spectra, densities and integrated densities of states, and dynamic-response functions for electron and phonon dynamics on the two-dimensional Penrose and Fibonacci quasicrystals. Certain special techniques have been developed for the investigation, such as the exact convolution relationship between dynamical quantities (i.e., densities and integrated densities of states and the dynamic-structure factor) of the two-dimensional Fibonacci lattices and those of the one-dimensional Fibonacci chains. An important consequence is that the dynamic-structure factor of the two- and three-dimensional Fibonacci superlattice is completed determined by that of the one-dimensional Fibonacci chain. In addition, the exact reduction of the dynamic-response function for the equal-coupling 2D Fibonacci quasilattice provides a useful interpretation of the unequal-coupling dispersion curves.

By comparing with dynamic properties for the principal one-dimensional systems investigated previously[15,16] (the Fibonacci chain) and between the two-dimensional system investigated here, certain characteristics and features can be seen to be common, and can be expected to occur in typical quasicrystals in higher dimensions also. These include the applicability of continuum viewpoints and results, for integrated densities of states (e.g., in phonon dynamics at low frequency) and for dynamic response ($\mathbf{q}$ small) making the IDOS proportional to $\omega^{d/2}$ in low-frequency phonon dynamics, and $S(\mathbf{q},\omega^2)\propto\delta[\omega^2-f(\mathbf{q})]$ at low $\mathbf{q}$ and $f(\mathbf{q})\sim|\mathbf{q}|$ in the isotropic limit. Other generally applicable features are the appearance of many gaps in the spectrum (plateaux in the IDOS) at sufficiently large values of appropriate coupling ratios, gap-labeling formulas, a complicated structure to the response function, and a symmetry in the $\mathbf{q}$ dependence of the response function $S(\mathbf{q},\omega^2)$ reflecting the n-fold symmetry of the quasicrystal ($n=4,2,2,5$ in the two-dimensional isotropic Fibonacci, anisotropic Fibonacci, periodically extended Fibonacci, and Penrose lattices, respectively).

The main spectral features which can differ qualitatively between one- and two-dimensional systems are the band number N and total bandwidth B and the form of the gap-labeling rules. In the Fibonacci chain N and B are (except for the equal-coupling case) infinite and zero, respectively, while in the two-dimensional periodically extended Fibonacci lattice both are finite. The 2D Fibonacci quasilattice is still more interesting in having two transitions between three regions (I, II, III) in which N,B can be both finite, or infinite and finite, or infinite and zero. The Penrose lattice has N finite, and so B is always nonzero. As for the one-dimensional Fibonacci-chain quasicrystal, the plateaux in the integrated density of states for the two-dimensional Fibonacci superlattice and quasilattice, as well as a particular two-dimensional Penrose lattice, can be labeled by integers. However, unlike the one-dimensional case, the largest gaps in the two-dimensional spectra do not correspond to the smallest integer values and will be explained in a future publication. We expect that all these types of behavior can occur in various higher-dimensional quasicrystalline models.

Equal-coupling limits can be trivial (e.g., for the densities of states of one- and two-dimensional Fibonacci lattices), simple enough to allow exact but nontrivial results to be obtained (e.g., for the response functions of one- and two-dimensional Fibonacci lattices), or very complicated, in the sense that no analytic simplifications occur and numerical computation is needed (Penrose lattice). It is again clear that examples of all of these types of situations can occur in various higher-dimensional models.

The present investigation therefore shows that a great variety of different dynamic behaviors will occur in higher-dimensional quasicrystals, unlike what is suggested by the previous detailed knowledge from the Fibonacci chain.

Further studies are desirable to provide a more detailed catalog of behaviors, to consider other dynamic properties, e.g., transport, and to address additional questions, such as the validity of a continuum limit, the effects of disorder on dynamics, and the relationship, if any, of the type of viewpoints used here to traditional methods for incommensurate systems.

ACKNOWLEDGMENTS

One of us (J.A.A.) is grateful to the Natural Sciences and Engineering Research Council of Canada for financial support. Part of this work has been done during visits of J.M.L. to the University of Oxford, where he received partial financial support from the French-British Prize Foundation. J.M.L. would like to thank J. Bellissard for useful discussions.

APPENDIX A: THE DECIMATION METHOD

The generating function approach provides an *a priori* exact means of computing lattice Green functions G_{ij} and, in particular, the average density or integrated density of states. This formalism is based on the following Gaussian generating function:[45,46]

$$\mathcal{I}_N(E)=\ln\Xi_N(E)\ , \tag{A1}$$

where

$$\Xi_N(E)=\int\mathcal{D}u\exp\left[\frac{i\mathcal{A}(E)}{2}\right.$$

with

$$\mathcal{A}(E)=\mathbf{U}^T[(E+i\eta)\mathbf{I}-\mathbf{H}]\mathbf{U} ,$$

$$\int \mathcal{D}u=\prod_{j=1}^{N}\int_{-\infty}^{\infty} du_j ,$$

and $\mathbf{U}$ denotes a column vector whose elements are the u_j. Note that the addition of the small positive imaginary part η to the spectral variable E is necessary for the convergence of the integrals. Changing variables to $\mathbf{V}=\mathbf{T}\mathbf{U}$, where $\mathbf{T}$ is the transformation which diagonalizes $\mathbf{H}$, it is straightforward to show that

$$N(E)\equiv\frac{1}{N}\sum_{\alpha}\Theta(E-E_\alpha)=\tfrac{1}{2}+\frac{2}{N\pi}\mathrm{Im}\mathcal{F}_N(E), \quad \text{(A2)}$$

$$\rho(E)\equiv\frac{1}{N}\sum_{\alpha}\delta(E-E_\alpha)=\frac{2}{N\pi}\mathrm{Im}\frac{\partial\mathcal{F}_N(E)}{\partial E} . \quad \text{(A3)}$$

In most cases it is not possible to find a transformation $\mathbf{T}$ which diagonalizes $\mathbf{H}$, and so, in the spirit of the renormalization group, we shall successively perform the Gaussian integrals over a fraction of the u_j ("decimation" of the sites they occupy). This leads at once to the relationship

$$\mathcal{F}_N(E;\{P_k\})=C(E;\{P_k\})+\mathcal{F}_{N/b}(E;\{P'_k\}) , \quad \text{(A4)}$$

where $\{P_k\}$ denotes the set of parameters characterizing the Hamiltonian $\mathbf{H}$ (i.e., exchange interactions, on-site energies, magnetic fields, etc.), $\{P'_k\}$ is the renormalized set of parameters, C is an additive term arising from completing the square in (A1), and b is the decimation rescaling factor. In the case of a Fibonacci chain, if we take the Hamiltonian $\mathbf{H}$ to be of the tight-binding form characterized by site energies ε_α, ε_β, and ε_γ which depend on the local environment, and nearest-neighbor hopping-matrix elements V_A and V_B, then one can show[47] that decimation of the β-type sites leads to

$$N(E)=\tfrac{1}{2}-\frac{1}{\pi}\sum_{n=1}^{\infty}\frac{1}{\tau^{n+1}}\mathrm{Im}\ln(E+i\eta-\varepsilon_\beta^{(n-1)})^{-1} , \quad \text{(A5)}$$

$$\rho(E)=\frac{-1}{\pi}\sum_{n=1}^{\infty}\frac{1}{\tau^{n+1}}\mathrm{Im}\frac{Q_\beta^{(n-1)}}{E+i\eta-\varepsilon_\beta^{(n-1)}} , \quad \text{(A6)}$$

where

$$Q_\beta^{(n)}=\frac{\partial(E-\varepsilon_\beta^{(n)})}{\partial E} .$$

Finally, the recursion relations for the parameters ε_j and V_{ij} are given by

$$\begin{aligned}
\varepsilon'_\alpha&=\varepsilon_\gamma+\frac{(V_A^2+V_B^2)}{E-\varepsilon_\beta} ,\\
\varepsilon'_\beta&=\varepsilon_\gamma+\frac{V_B^2}{E-\varepsilon_\beta} ,\\
\varepsilon'_\gamma&=\varepsilon_\alpha+\frac{V_A^2}{E-\varepsilon_\beta} , \quad \text{(A7)}\\
V'_A&=\frac{V_AV_B}{E-\varepsilon_\beta} ,\\
V'_B&=V_A .
\end{aligned}$$

APPENDIX B: CONVOLUTION OF TWO CANTOR SETS

The transitions between finite and infinite band number, and between finite and zero bandwidth, can be illustrated by considering the simpler example of the convolution of two identical Cantor sets.

If $R_{\lambda,\mu}$ (with $\lambda+\mu<1$) is the operator taking any interval $[a,b]$ into the union of the two intervals $[a,a+\lambda(b-a)]$, $[b-\mu(b-a),b]$, we define I_1 as the asymmetric Cantor set obtained as the $n\to\infty$ limit of the sequence

$$I_1^{(n)}=(R_{\lambda,\mu})^n[0,1] . \quad \text{(B1)}$$

This set is, at the nth stage, actually the union of 2^n nonoverlapping elementary intervals, whose total width (Lebesgue measure) is $(\lambda+\mu)^n$. So the limit set $I_1=\lim_{n\to\infty}I_1^{(n)}$ is a Cantor set with infinite band number and zero width. We can consider now the set I_2 defined as the limit as $n\to\infty$ of the convolution $I_2^{(n)}$ of $I_1^{(n)}$ with itself.

We first consider the simple case where the Cantor set I_1 is symmetric, obtained by setting $\mu=\lambda$. Then it is easy to show using (B1) and the convolution relation that $I_2=\lim_{n\to\infty}I_2^{(n)}$, where

$$I_2^{(n+1)}=S_\lambda I_2^{(n)} \quad \text{(B2)}$$

with $I_2^{(0)}=[0,2]$ and where S_λ takes any interval $[a,b]$ into the union of the three intervals $[a,a+\lambda(b-a)]$, $[a+\frac{1}{2}(1-\lambda)(b-a),a+\frac{1}{2}(1+\lambda)(b-a)]$, $[b-\lambda(b-a),b]$. These three intervals are nonoverlapping if $\lambda<\frac{1}{3}$ and overlapping (so their union is the whole interval $[a,b]$) if $\lambda>\frac{1}{3}$. So $\lambda=\frac{1}{3}$ divides the regime $\lambda<\frac{1}{3}$ in which the band number N and total width B are infinite and zero (I_2 is a Cantor set with zero measure), from that ($\lambda>\frac{1}{3}$) in which $N=1$ and $B=2$ are finite, since $I_2=[0,2]$. These are the two phases III and I, respectively, of Sec. II A, and the transition at $\lambda=\frac{1}{3}$ joins them with no intermediate phase II in this case.

To see the appearance of phase II, it is necessary to take the general, asymmetric model ($\lambda\neq\mu$). For this case, no simple equation of type (B2) can apply. A pictorial reason for this is given in Fig. 23. In Figs. 23(a)

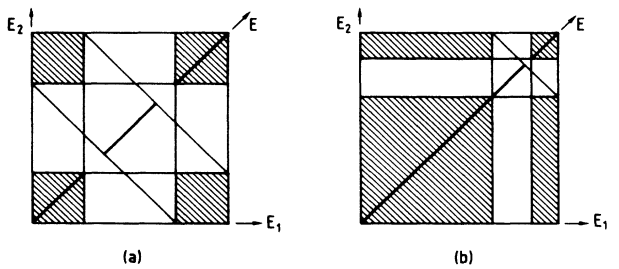

FIG. 23. Convolution of two Cantor sets: (a) for the symmetric case $\mu=\lambda<\frac{1}{3}$ (in phase III); (b) for the asymmetric case $\lambda=\frac{2}{3},\mu=\frac{2}{15}$ (in phase II). In both cases, only the first generation ($n=1$) is illustrated.

and 23(b) the abscissa and ordinate play the role of E_1 and E_2 in the convolution equation (2.3). The subdivision of the interval [0,1] along each axis is that provided by $R_{\lambda,\mu}$ as defined above. In Fig. 23(a) this is a symmetric subdivision ($\lambda=\mu$), and in Fig. 23(b) it is asymmetric. Projections from any point (E_1,E_2) in the plane onto the diagonal line parametrized by E (ranging from 0 to 2) arrive at $E=E_1+E_2$. The shaded parts of the plane are those in which both E_1 and E_2 belong to I_1, i.e., both $\rho_1^{(1)}(E_1)$ and $\rho_1^{(1)}(E_2)$ are nonzero. The process given in (B2) thus implies that in Fig. 23(a), $I_2^{(1)}$ is the projection onto the diagonal line of the shaded regions of the figure. Obviously, at higher n each shaded square subdivides as the whole square has done previously, and (B2) is a mathematical expression of this. However, in the asymmetric case [Fig. 23(b)] the shaded regions (again shown for the generation $n=1$) are distorted versions of those occurring in the previous generation, and this affects their projection in a highly nontrivial way. The parameter values λ,μ in Fig. 23(b) are such that it is plausible that continuing to higher n will leave a finite total width (total length of projected regions, shown for $n=1$ as a heavy line along the diagonal), while continuing to introduce more and more gaps in the top right-hand corner of the square. This is, in fact, so: the parameter values are such that B is finite and N infinite, corresponding to phase II, and thus all three phases appear in the model. It is interesting to note that in the descriptions just used, the problem has become that of projecting a fractal with no uniform scaling law.

We now present a more quantitative, albeit incomplete, study of the three phases. We define for further reference the sets

$$J^{(n)}(\alpha)=\frac{1}{\alpha+1}(I_1^{(n)}+\alpha I_1^{(n)}),$$

where α is an arbitrary scaling factor, and the usual definition of the (pointwise) sum of two sets is used. The definition (B1) shows that $J^{(n+1)}(\alpha)$ is the union of the following four sets: $\alpha J^{(n)}(\alpha)$, $1-\mu+\mu J^{(n)}(\alpha)$,

$$\frac{\alpha(1-\mu)}{\alpha+1}+\frac{\lambda+\alpha\mu}{\alpha+1}J^{(n)}\left[\frac{\alpha\mu}{\lambda}\right],$$

and

$$\frac{1-\mu}{1+\alpha}+\frac{\alpha\lambda+\mu}{1+\alpha}J^{(n)}\left[\frac{\alpha\lambda}{\mu}\right].$$

Moreover, $I_2^{(n)}=2J^{(n)}(1)$.

It can be shown that phase I is exactly given by the inequalities: $2\lambda+\mu\geq 1$; $\lambda+2\mu\geq 1$. Indeed, it is easy to prove by recursion that

$$J^{(n)}(1)=J^{(n)}\left[\frac{\lambda}{\mu}\right]=J^{(n)}\left[\frac{\mu}{\lambda}\right]=[0,1]$$

if both above inequalities hold, and that the band number N diverges with the iteration label n if either of those inequalities is violated. The boundary between phases II and III is much more difficult to locate in an exact way. A set of recursive inequalities for the widths $B^{(n)}(\alpha)$ of the sets $J^{(n)}(\alpha)$ can be derived, which shows, in particular, that $B^{(n)}(1)$ is bounded by $(\lambda^{1/2}+\mu^{1/2})^{2n}$. Hence, phase III contains at least the region defined by $\lambda^{1/2}+\mu^{1/2}\leq 1$. This lower bound for phase III intersects the bissectrix at $\lambda=\mu=\frac{1}{4}$, whereas the transition is known to occur for $\lambda=\mu=\frac{1}{3}$. It is quite possible that the actual boundary between phases II and III exhibits a richer structure than a single smooth curve.

[1]D. Shechtman, I. Blech, D. Gratias, and J. W. Cahn, Phys. Rev. Lett. **53**, 1951 (1984).

[2]D. Levine and P. J. Steinhardt, Phys. Rev. Lett. **53**, 2477 (1984).

[3]P. J. Steinhardt and S. Ostlund, *The Physics of Quasicrystals* (World-Scientific, Singapore, 1987).

[4]C. Godrèche, J. M. Luck, and H. Orland, J. Stat. Phys. **45**, 777 (1986).

[5]Y. Achiam, T. C. Lubensky, and E. W. Marshall, Phys. Rev. B **33**, 6460 (1986).

[6]J. M. Luck, J. Phys. A **20**, 1259 (1987).

[7]J. M. Luck and Th. M. Nieuwenhuizen, Europhys. Lett. **2**, 257 (1986).

[8]R. B. Stinchcombe, J. Phys. A **20**, L251 (1987).

[9]M. Kohmoto, L. P. Kadanoff, and C. Tang, Phys. Rev. Lett. **50**, 1870 (1983).

[10]S. Ostlund and R. Pandit, Phys. Rev. B **29**, 1394 (1984).

[11]J. M. Luck and D. Petritis, J. Stat. Phys. **42**, 289 (1986).

[12]J. P. Lu, T. Odagaki, and J. L. Birman, Phys. Rev. B **33**, 4809 (1986).

[13]M. Kohmoto, B. Sutherland, and C. Tang, Phys. Rev. B **35**, 1020 (1987).

[14]S. Evangelou, J. Phys. C **20**, L295 (1987).

[15]J. A. Ashraff and R. B. Stinchcombe, Phys. Rev. B **37**, 5723 (1988).

[16]J. A. Ashraff and R. B. Stinchcombe, Phys. Rev. B **39**, 2670 (1989).

[17]R. Penrose, Math. Intell. **2**, 32 (1979).

[18]R. M. Robinson (unpublished).

[19]B. Grünbaum and G. C. Shephard, *Tilings and Patterns* (Freeman, New York, 1986).

[20]R. Merlin, K. Bajema, R. Clarke, F.-Y. Juang, and P. K. Bhattacharya, Phys. Rev. Lett. **55**, 1768 (1985).

[21]K. Ueda and H. Tsunetsugu, Phys. Rev. Lett. **58**, 1272 (1987).

[22]W. A. Schwalm and M. K. Schwalm, Phys. Rev. B **37**, 9524 (1988).

[23]T. C. Choy, Phys. Rev. Lett. **55**, 2915 (1985).

[24]T. Odagaki and D. Nguyen, Phys. Rev. B **33**, 2184 (1986).

[25]M. Kohmoto and B. Sutherland, Phys. Rev. Lett. **56**, 2740 (1986).

[26]M. Kohmoto and B. Sutherland, Phys. Rev. B **34**, 3849 (1986).

[27]H. Tsunetsugu, T. Fujiwara, K. Ueda, and T. Tokihiro, J. Phys. Soc. Jpn. **55**, 1420 (1986).

[28]V. Kumar and G. Athithan, Phys. Rev. B **35**, 906 (1987).

[29]N. Nishiguchi and T. Sakuma, Phys. Rev. B **38**, 7370 (1988).
[30]D. Levine and P. J. Steinhardt, Phys. Rev. B **34**, 82 (1986).
[31]A. Sütő (unpublished).
[32]B. Sutherland, Phys. Rev. B **34**, 3904 (1986).
[33]T. Tokihiro, T. Fujiwara, and M. Arai, Phys. Rev. B **38**, 5981 (1988).
[34]B. Simon, Adv. Appl. Math. **3**, 463 (1982).
[35]J. Bellissard, in *Statistical Mechanics and Field Theory: Mathematical Aspects,* Vol. 257 of *Lecture Notes in Physics* (Springer, Berlin, 1986).
[36]V. Elser, Phys. Rev. B **32**, 4892 (1985).
[37]A. Katz and M. Duneau, J. Phys. (Paris) **47**, 181 (1986).
[38]J. E. S. Socolar, P. J. Steinhardt, and D. Levine, Phys. Rev. B **32**, 5547 (1985).
[39]F. Gähler and J. Rhyner, J. Phys. A **19**, 267 (1986).
[40]M. Gardner, Sci. Am. **236**, 110 (1977).
[41]D. Levine, J. Phys. (Paris) **46**, C8-397 (1985).
[42]R. B. Stinchcombe (unpublished).
[43]R. Alben, S. Kirkpatrick, and D. Beeman, Phys. Rev. B **15**, 346 (1977).
[44]H. Patel and D. Sherrington, Phys. Rev. B **40**, 11 185 (1989).
[45]A.-M. S. Tremblay and B. W. Southern, J. Phys. Lett. **44**, L843 (1983).
[46]M.-A. Lemieux and A.-M. S. Tremblay, Phys. Rev. B **36**, 1463 (1987).
[47]J. A. Ashraff, D. Phil. thesis, Oxford, 1989.

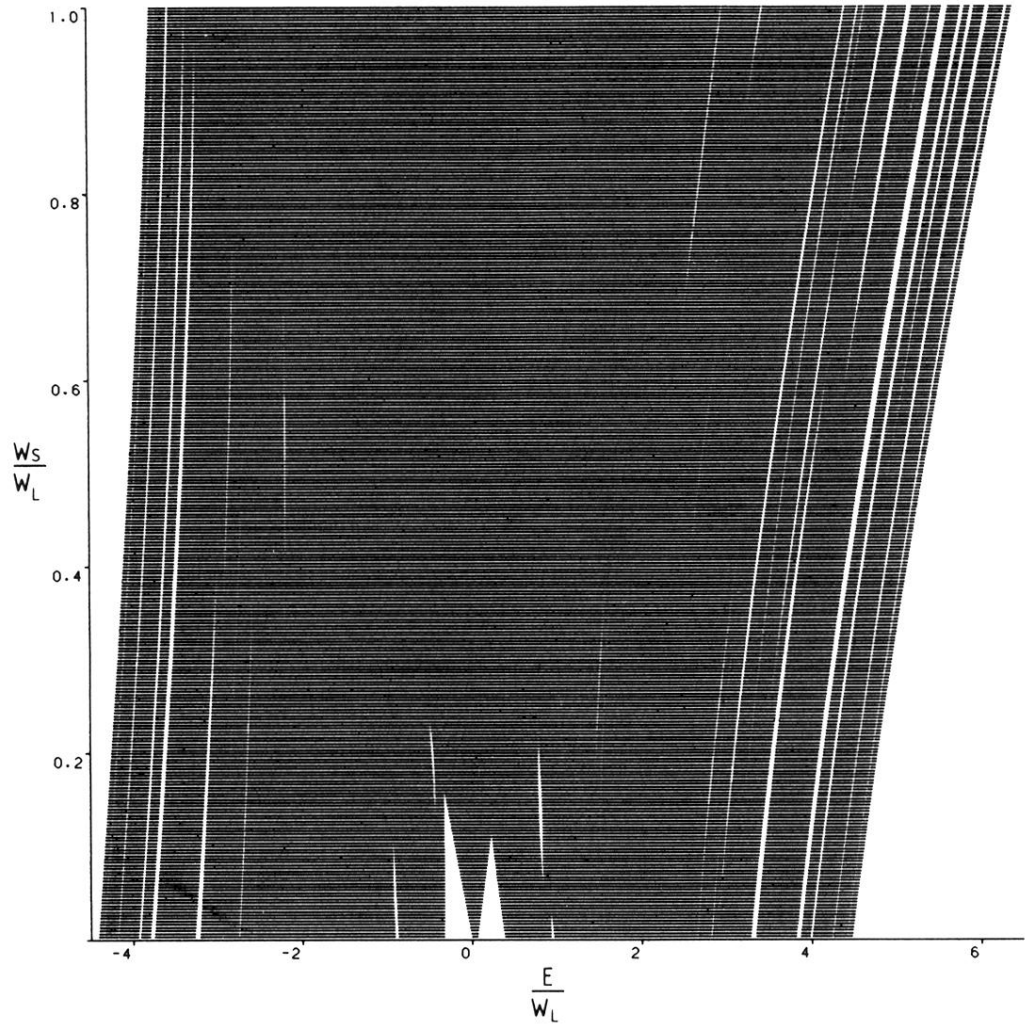

FIG. 15. The energy spectrum for a 2D Penrose lattice composed of Robinson tiles, consisting of 539 sites ($0 \leq W \leq 1$).

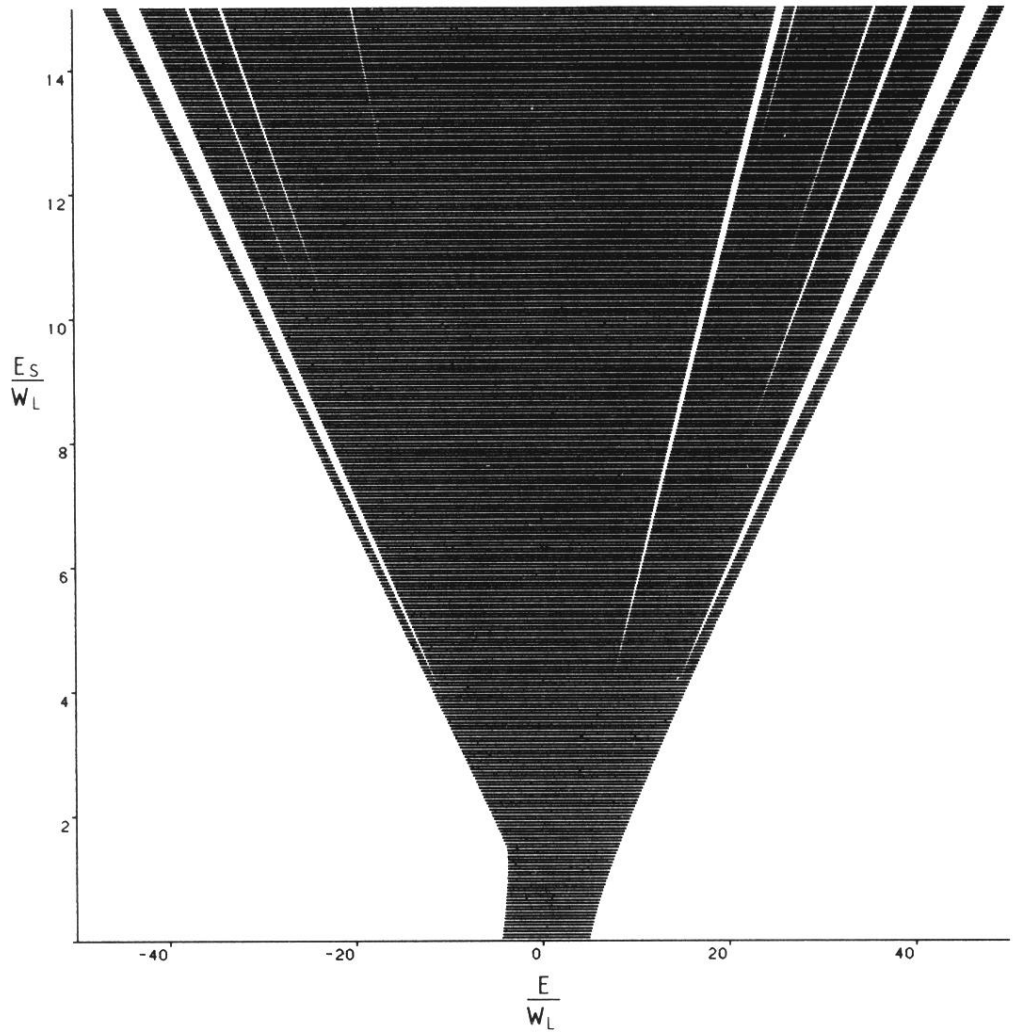

FIG. 16. The energy spectrum for a 2D Penrose lattice composed of Robinson tiles, consisting of 539 sites ($0 \leq W \leq 10$).

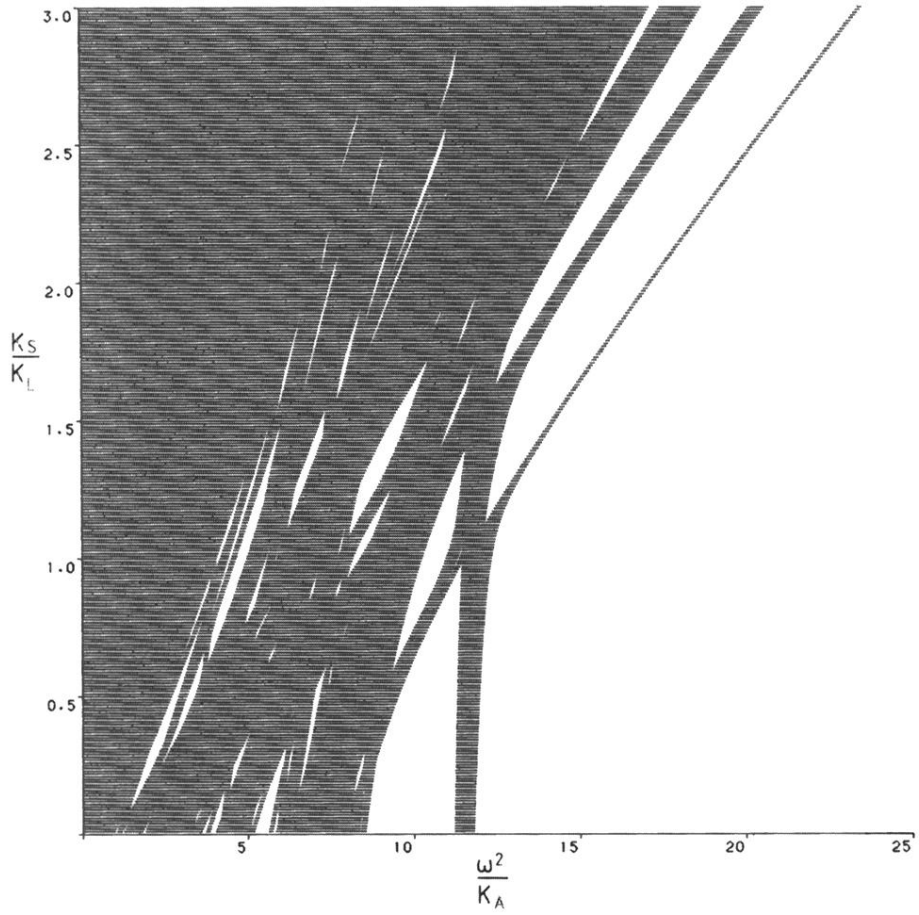

FIG. 17. The frequency spectrum for a 2D Penrose lattice composed of Robinson tiles, consisting of 539 sites ($0 \leq K \leq 3$).

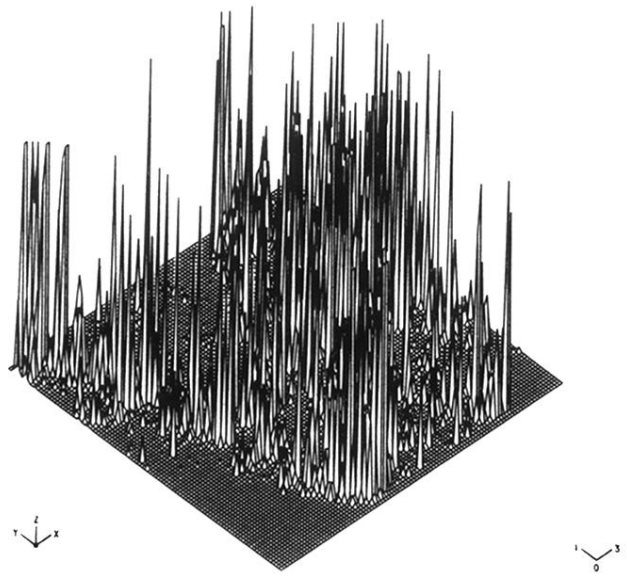

FIG. 18. A surface plot of $S(\mathbf{q},\mathrm{E})$ for electron dynamics on the isotropic Fibonacci square lattice for $\mathbf{q}$ in the (1,1) direction and $W_A=1$, $W_B=2$. The x axis corresponds to q for $0\leq q\leq 2\pi$ and the y axis to E/W_A for $-6\leq E/W_A\leq 6$.

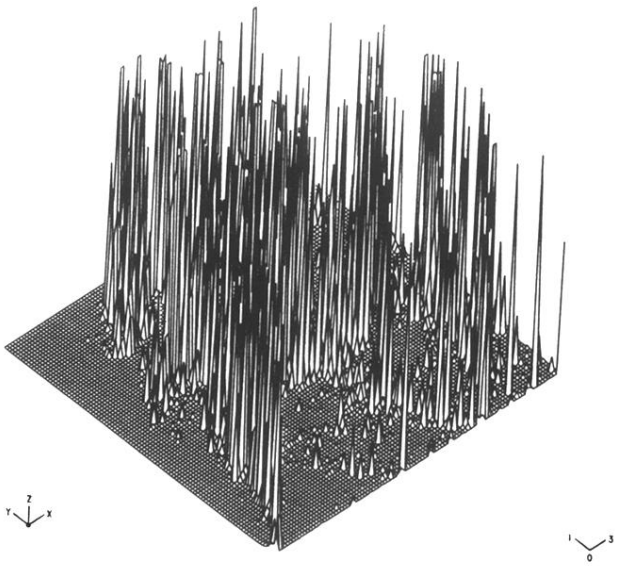

FIG. 19. A surface plot of $S(\mathbf{q},\omega^2)$ for phonon dynamics on the isotropic Fibonacci square lattice for $\mathbf{q}$ in the (1,1) direction and $K_A=1$, $K_B=2$. The x axis corresponds to q for $0\leq q\leq 2\pi$ and the y axis to ω^2/K_A for $0\leq\omega^2/K_A\leq 12$.